

THz RADIATION DIAGNOSTICS FOR MONITORING THE BUNCH COMPRESSION AT THE SwissFEL INJECTOR TEST FACILITY

Ch. Gerth*, B. Schmidt, S. Wesch, DESY, D-22603 Hamburg, Germany
R. Ischebeck, G.L. Orlandi, P. Peier, V. Schlott, PSI, CH-5232 Villigen, Switzerland

Abstract

At the SwissFEL Injector Test Facility, installation of a magnetic chicane for longitudinal bunch compression is foreseen for the first half of 2011. Bunch compression will be accomplished by operating two S-band accelerating structures on-crest and two S-band structures at off-crest RF phases. An X-Band structure for the linearization of the longitudinal phase space will be installed at a later stage. The detection of coherent synchrotron radiation or coherent diffraction radiation in the THz range can be used to monitor the bunch compression process and stabilize the RF phases by a beam-based feedback. In this paper, we study the source characteristics of diffraction radiation generated by a metallic foil with a hole. The performance of a bunch compression monitor consisting of a focusing mirror and detector has been evaluated by simulating the THz radiation transport of the optical components. Particle tracking simulations were used to model the bunch compression process for different operation modes.

INTRODUCTION

At the Paul Scherrer Institute, a 250 MeV Injector Test Facility [1] is currently being commissioned in order to demonstrate the capability of generating the beam properties [2] envisaged for SwissFEL [3], a linac-driven X-ray free-electron laser (FEL) operating in the wavelength range 0.1–7 nm. The test facility is equipped with a 2.6-cell S-band photo-cathode RF gun followed by four S-Band normal conducting travelling wave structures and a fourth harmonic X-Band structure for phase space linearization. Longitudinal bunch compression is realized by a 10.5 m long magnetic chicane which consists of four dipoles and two quadrupoles for dispersion correction. The nominal bending angle range is $3.0^\circ - 5.0^\circ$ with corresponding R_{56} of 25 mm – 69 mm, respectively. A dedicated diagnostic section [4] has been installed after the bunch compressor for the characterization of the transverse and longitudinal beam properties.

A simple and non-invasive method to monitor the longitudinal bunch compression process is the diagnosis of coherent diffraction radiation (CDR) which is generated by an electron bunch passing a metallic surface with an opening. The spectral density distribution radiated by a bunch of N electrons is given by

$$\frac{d^2U}{d\lambda d\Omega} = \left(\frac{d^2U}{d\lambda d\Omega} \right)_1 (N + N(N-1) \cdot |F(\lambda, \Omega)|^2), \quad (1)$$

* Permanent address: DESY Hamburg, christopher.gerth@desy.de

Table 1: Injector Test Facility Parameters

| Parameter | Unit | Mode 1 | Mode 2 |
|--------------------|------|--------|--------|
| Bunch charge | pC | 200 | 10 |
| Beam energy | MeV | 250 | 250 |
| Bunch length (rms) | fs | 300 | 87 |
| Peak Current | A | 266 | 45 |

where $(d^2U/d\lambda d\Omega)_1$ is the single electron spectrum and F the bunch form factor. For the test facility beam parameters given in Table 1, transverse beam size effects can be neglected [5] and the longitudinal bunch form factor can be applied in good approximation.

The longitudinal bunch form factor is given by the Fourier transform of the longitudinal charge distribution and defines the corresponding wavelength range for which coherent emission occurs. The magnitude of the longitudinal bunch form factor for both the 200 pC and 10 pC mode are plotted in Fig. 1. As can be seen, a bunch compression monitor (BCM) based on CDR for the test facility needs to be capable of producing, transporting and detecting radiation in the range of about $50 \mu\text{m} - 1 \text{ mm}$.

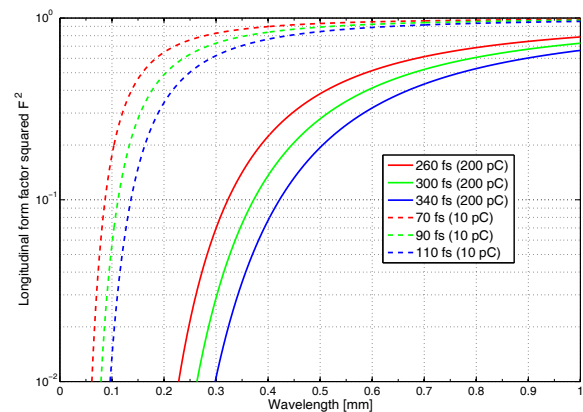


Figure 1: Square of the longitudinal bunch form factor for the 200 pC (solid) and 10 pC (dashed) mode.

SIMULATION SETUP

For the modelling of the BCM we assume that a diffraction radiator is mounted to a screen holder of an existing profile monitor [4] at an angle of 45° w.r.t. the electron beam axis. The broad-band THz radiation can be extracted through a CF40 vacuum window opposite to the direction

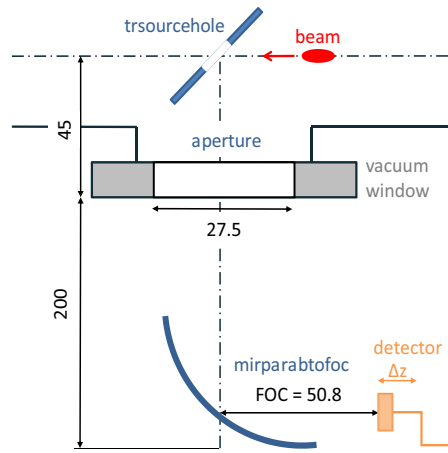


Figure 2: Schematic of the BCM for optics simulations.

for transverse profile measurements. A parabolic mirror ($f = 50.8$ mm, diameter 2 inch) is then used to focus the radiation onto the detector. A schematic with the dimensions of the BCM is depicted in Fig. 2. As for wavelengths longer than $1 \mu\text{m}$ near-filed diffraction has to be applied [6], the emission and transport of the radiation was modeled with the *Mathematica* package *THzTransport*, and the module names of *THzTransport* used for the modelling have been included in Fig. 2.

The size of the opening of the diffraction radiator for the electron beam defines the cut-off at short wavelengths of the CDR. In the left part of Fig. 3, the spectral density distributions at the vacuum window emitted from rectangular screens ($30 \times 30 \text{ mm}^2$) with hole diameters of 6 mm and 10 mm are compared. The relative ratio of both curves is shown in the right part of Fig. 3. For wavelength shorter than $100 \mu\text{m}$ the intensity for the hole diameter of 10 mm decreases by more than 50% compared to the hole diameter of 6 mm. Whereas a smaller hole diameter produces more intensity at short wavelengths, it makes beam steering more sensitive and generates more wakefields. It has also been found that for a vacuum window with an aperture of 27.5 mm diameter (typical window size for a CF40 flange)

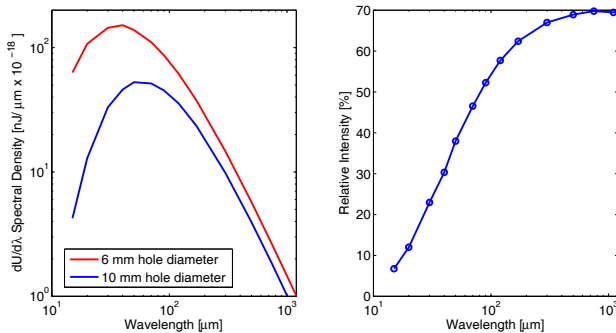


Figure 3: Left: Single electron DR spectrum for hole diameters of 6 mm and 10 mm. Right: Intensity ratio of the curves in the left plot.

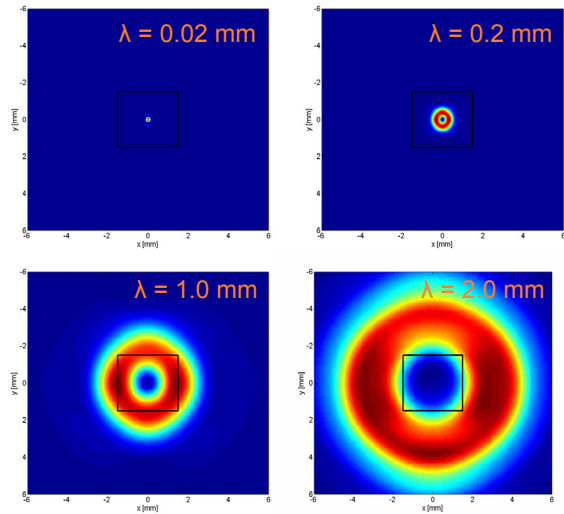


Figure 4: Transverse intensity profiles in the focal plane for different wavelengths. Typical detector size of $3 \times 3 \text{ mm}^2$ is indicated by a black square.

more than 80% of the total radiation up to a wavelength of $\lambda = 3 \text{ mm}$ is transmitted.

Figure 4 shows the intensity profile of both polarizations in the focal plane of the parabolic mirror for the wavelengths $\lambda = 0.02 \text{ mm}$, 0.2 mm , 1 mm and 2 mm . A square of $3 \times 3 \text{ mm}^2$ has been included in the images to illustrate a typical size of a detector surface area. For wavelengths $\lambda < 1 \text{ mm}$ most of the intensity is confined in the square of $3 \times 3 \text{ mm}^2$, whereas in the case of $\lambda = 2 \text{ mm}$ most of the intensity is distributed around the square due to the vanishing intensity in the centre caused by the radial polarization of diffraction radiation. This effect can be mitigated by slightly displacing the detector in the transverse plane.

As the radiation is slightly divergent and not emitted as a

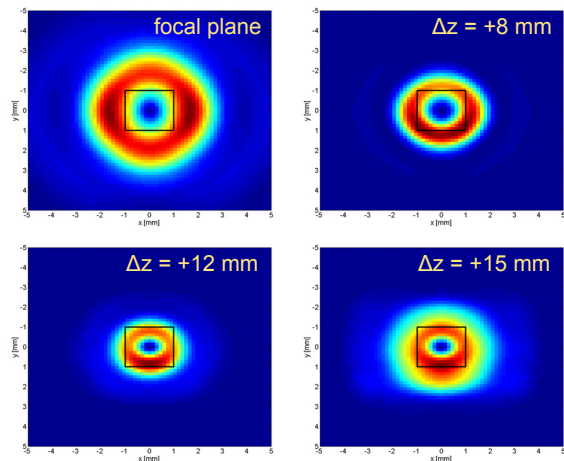


Figure 5: Transverse intensity profiles at $\lambda = 1 \text{ mm}$ for different longitudinal detector positions Δz .

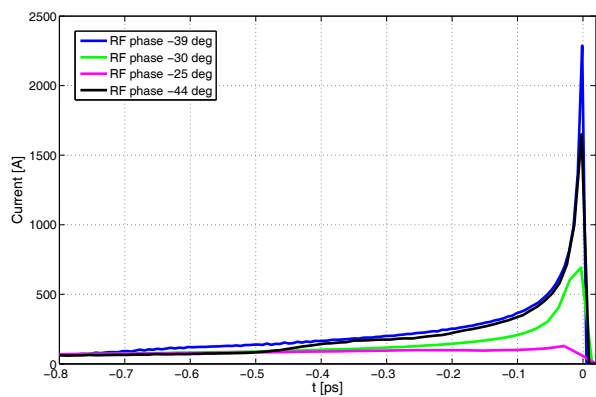


Figure 6: Longitudinal bunch profiles for different RF phase settings and a bunch charge of 200 pC.

plane wave from the diffraction radiator, the minimum spot size is found slightly behind the focal plane of the parabolic mirror. This is demonstrated in Fig. 5 for four longitudinal detector positions Δz at a wavelength of $\lambda = 1$ mm: the minimum spot size was found at $\Delta z = +12$ mm. The optimum detector position can be determined experimentally by positioning the detector with the help of a motorized linear stage for highest intensity.

RF PHASE SCAN

After installation of the bunch compressor, the fourth harmonic X-Band structure for phase space linearization will not be available immediately. Bunch compression will be realized by operating the first two accelerating structures on-crest and third and fourth structure, which share one klystron, at off-crest RF phases to introduce the required energy chirp. The particle tracking code *elegant* [7] has been used to model the bunch compression process, and the longitudinal charge distributions for various RF phase settings and a bunch charge of 200 pC are shown in Fig. 6. The charge distribution exhibit an asymmetric shape due to the sonisoidal shape of the RF.

THzTransport has been used to estimate the total radiated energy at the position of the detector (see Fig. 2) integrated over the wavelength range $50 \mu\text{m} - 3$ mm. As a diffraction radiator, a rectangular screen ($30 \times 30 \text{ mm}^2$) with a hole diameter of 6 mm was assumed. Absorption in air or in the vacuum window material as well as a finite detector size were not taken into account. The charge profiles from the particle tracking were used to calculate the longitudinal bunch form factors for different RF phase settings. The total radiated energy as a function of the RF phase is shown in Fig. 7. The maximum of the RF phase scan occurs at a phase of -39 deg with respect to on-crest. Such an RF phase scan can be used as a fast and simple method to setup the absolute RF phase of the third and fourth accelerating structure.

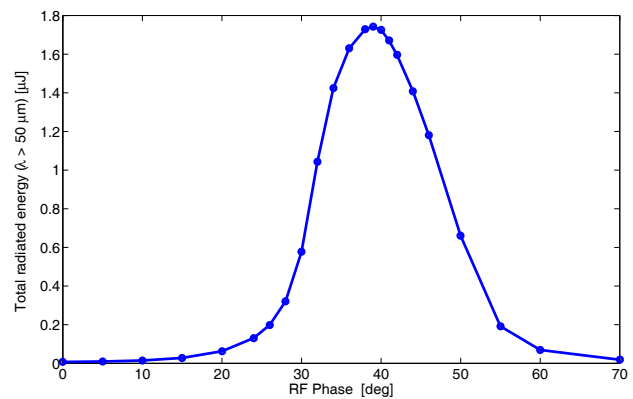


Figure 7: Total radiated energy during RF phase scan for a bunch charge of 200 pC.

CONCLUSIONS AND OUTLOOK

The source characteristics of CDR and a simple setup for a BCM for THz diagnostics have been studied for the operating modes of the 250 MeV Injector Test Facility at PSI. A titanium foil with a hole diameter of 6 mm has been chosen as a diffraction radiator and installed at a profile monitor station [4] immediately after the BC and before an RF deflector. At the moment, the application of beam splitters and bandpass filters for an enhanced performance of the BCM for different operating conditions and the optimum choice for a THz detector, e.g. pyro-electric detector or THz antenna, are under study.

ACKNOWLEDGEMENTS

The authors are grateful to E. Prat and S. Reiche for their support with the particle tracking simulations. This work is partly supported by IRUVX-PP an EU co-funded project under FP7 (Grant Agreement 211285).

REFERENCES

- [1] M. Pedrozzi (ed.), “250 MeV Injector Conceptual Design Report”, PSI Bericht 10-05 (2010).
- [2] M. Pedrozzi *et al.*, “250 MeV Injector Facility for the Swiss-FEL Project”, FEL’09, Liverpool, TUPC38.
- [3] R. Ganter (ed.), “SwissFEL Conceptual Design Report”, PSI Bericht 10-04 (2010).
- [4] R. Ischebeck *et al.*, “Profile Monitors for the SwissFEL Injector Test Facility”, LINAC10, Tsukuba, TUP103.
- [5] O. Grimm *et al.*, “Transverse Electron Beam Size Effect on the Bunch Profile Determination with Coherent Radiation Diagnostics”, EPAC’08, Genoa, TUPC030.
- [6] S. Casalbouni *et al.*, “Far-Infrared Transition and Diffraction Radiation, Part I: Production, Diffraction Effects and Optical Propagation”, TESLA Report 2005-15, 2005.
- [7] M. Borland, “*elegant*: A Flexible SDDS-Compliant Code for Accelerator Simulation”, Advanced Photon Source LS-287, 2000.